



HAL
open science

Strategies for selective functionalization of amorphous chalcogenide rib waveguides

Bruno Robert, Rémi Pélissier, Raphaël Escalier, Ahmad Mehdi, Csilla Gergely, Caroline Vigreux

► **To cite this version:**

Bruno Robert, Rémi Pélissier, Raphaël Escalier, Ahmad Mehdi, Csilla Gergely, et al.. Strategies for selective functionalization of amorphous chalcogenide rib waveguides. *Optical Materials*, 2022, 127, pp.112327. 10.1016/j.optmat.2022.112327 . hal-03642344

HAL Id: hal-03642344

<https://hal.science/hal-03642344>

Submitted on 22 Jul 2024

HAL is a multi-disciplinary open access archive for the deposit and dissemination of scientific research documents, whether they are published or not. The documents may come from teaching and research institutions in France or abroad, or from public or private research centers.

L'archive ouverte pluridisciplinaire **HAL**, est destinée au dépôt et à la diffusion de documents scientifiques de niveau recherche, publiés ou non, émanant des établissements d'enseignement et de recherche français ou étrangers, des laboratoires publics ou privés.



Distributed under a Creative Commons Attribution - NonCommercial 4.0 International License

Strategies for selective functionalization of amorphous chalcogenide rib waveguides

Bruno Robert^{1,2}, Rémi Pélissier³, Raphaël Escalier¹, Ahmad Mehdi¹, Csilla Gergely² and Caroline Vigreux^{*1}

¹ ICGM, Univ. Montpellier, CNRS, ENSCM, Montpellier, France

² L2C, Univ. Montpellier, CNRS, Montpellier, France

³ PHIM, CEFÉ, Institut Agro, INRAE, CIRAD, Univ. Montpellier, Montpellier, France

Keywords: Chalcogenide films, waveguides, selective functionalization, wettability, fungi spore immobilization

Abstract

We report on two selective functionalization strategies to create a chemical contrast between the active rib waveguides and the passive surrounding areas of a chalcogenide-based optical sensing system. In such configuration, the analyte could be concentrated on the waveguides and interact with the evanescent field, producing a stronger optical signature. The rib waveguides are obtained by photolithography and subsequent ion beam etching of amorphous Ge-Se-Te thin films that allow residual resist to remain above the waveguides. The first functionalization strategy consists in the reuse of the resist as a mask during the following surface modification process. It allows the functionalization of all areas around the waveguides. The second strategy consists of depositing a new sacrificial metal layer, leading to a perfect negative functionalization contrast, modifying only the waveguides. For the two strategies developed, three precursors were used. The use of a silylated fluorescein derivative allowed the validation of the protocols, with the observation of a fluorescence contrast between the functionalized and non-functionalized areas. The use of tetraethoxysilane as a hydrophilic precursor and the mixture of tetraethoxysilane and octyl-trimethoxysilane as a hydrophobic precursor created a clear contrast in wettability between the rib waveguides and the surrounding areas. A spore deposition was performed on functionalized components according to the two proposed strategies, with the two hydrophilic/hydrophobic precursors. The spore immobilization rate was increased by making the waveguides more hydrophobic, as well as by making the areas surrounding the guides more hydrophilic, demonstrating the effectiveness of our two strategies.

1. Introduction

The need for optical remote sensors for *in situ* diagnosis of diseases, monitoring industrial process and detection of environmental pollutants is playing an important role in the development of miniaturized infrared optics. Chalcogenide-based optical waveguides express advantageous properties in the development of infrared bio-chemical sensors [1;2]. Thanks to their high refractive index and glassy structure, amorphous chalcogenide films can be easily integrated in a “lab-on-a-chip” microsystem platform, built up along with a light source and a photodetector [3-5]. Their wide transparency window makes them suitable for application in both near-infrared range [6-8] and mid-infrared range [9-11]. Depending on the waveguiding structures, a little portion of the light propagates outside of the core material. This evanescent field is likely to probe the external environment, and therefore to allow to collect information about analytes presence, structure, or concentration [12]. Most of those waveguiding structures are built by a technology comprising two main steps which are lithography and etching, leading to channel waveguides. Channel waveguides can be characterized by different geometries; one example is the rib structure [13-15], in which the core layer is partially etched in a rectangular or trapezoidal profile, depending on the angle of attack of the etching.

In bio-chemical sensors based on optical rib waveguides, the signal transduction i.e., the capture of molecules, can be based either on refractometric or spectroscopic techniques. Refractometric techniques request biofunctionalized chalcogenide waveguides, where the specific adsorption of the analytes is monitored as the consecutive alteration of the effective index of the propagating mode [16;17]. So far as our knowledge, all the waveguide functionalization processes described in literature are operated in a full-sheet manner. Thus, meaning that both the waveguide and the supporting chip surfaces are modified with the same specific capturing reagent. Hence, the analytes could either adsorb on the active sensing part or onto the inert substrate.

On the other hand, most of the detection principles of chalcogenide waveguides are based on spectroscopic techniques. The analytes depositing on the waveguide generate a specific absorption of the evanescent infrared light, rendering the chalcogenide waveguide promising in remote spectroscopy-based sensing. Moreover, working in the near infrared range [0.8-2.5 μm] opens the possibility for complex integrated devices, taking advantage of the low-cost optical components developed for the telecommunication bands, such as light sources (LEDs, gas and solid-state laser) and detectors. Previous studies already demonstrated optical detection in the IR domain of chloroform at 1.69 μm [7], phenylethylamine at 1.51 μm [6], or water at 1.45 μm [8]. Other studies demonstrated biosensing in the mid IR region [5;18;19], where the main signatures of molecules and biomolecules are located. The absorption within the evanescent field follows a pseudo-Lambert–Beer relationship:

$$A = (\varepsilon \cdot c \cdot r) \times \ell$$

where ε is the molar absorptivity, c is the concentration of the analyte, r is the fraction of the evanescent power and ℓ is the optical path length. To enhance sensitivity, authors propose to increase the optical path length, by designing spiral structures [5;18;20] or “snake” patterns [21], covering the whole detection surface. Nevertheless, non-straight and longer structures come along with higher optical losses, already reported as regular limitations of chalcogenide waveguides [22;23].

The two detection techniques are based on the presence of an analyte within the evanescent field of the guiding structure. To enhance sensitivity, we propose to selectively functionalize the transducing surface. Such functionalization aims to provide a chemical contrast between rib waveguides and the surrounding surface. Therefore, when molecules, proteins or particles of interest adsorb only on the waveguide, they are sensed by the evanescent field and all of them would participate in the transducing event. In order to provide such chemical contrast, we propose two different functionalization strategies. The first one consists in modifying the area surrounding the waveguides, aiming to avoid or at least limit adsorption of analytes on this area. This process preserves light propagation from being disrupted by any other add-layer on the top of the waveguide. The second strategy consists in modifying the active area only, being the waveguide. Such a specific recognition pattern would ensure that analytes are only adsorbed on the waveguide and hence contribute all to the sensor response. In both cases, the geometry of the core layer is modified by photolithography and ion beam etching and the proposed strategies to achieve a selective functionalization include the re-use of the lithography photoresist. Indeed, the residual resin after etching can be used to mask the areas that need to remain unchanged during the functionalization step. It should be noted that if amorphous chalcogenide thin films have been used, the processes are easily transposable to waveguides based on different materials or geometries, as soon as they are manufactured by lithography and etching.

Functionalization has been processed by silanization of the Ge-Se-Te surface using three different organosilane precursors. The first organosilane carries a fluorescent function that allows direct monitoring of the functionalized surfaces after the modification processes. Then two others organosilane were used to achieve wettability contrast on the surface (one rendering the surfaces more hydrophilic, the other making them more hydrophobic). These modified surfaces with an adequate wettability contrast have been tested against fungi spore deposition. Spores, micrometric capsules, responsible for the transmission of fungal diseases of plants, are indeed more easily immobilized on hydrophobic surfaces [24]. We thus compared the immobilized spore rates for the different functionalized surfaces according to one or the other strategy, and according to the precursor used.

2. Materials and Methods

2.1. Processes used to selectively functionalize specific areas

The Ge-Se-Te rib waveguide fabrication has been previously reported [11]. Basically, the waveguiding structures are composed from a silicon substrate, a $6\mu\text{m}$ -thick amorphous $\text{Ge}_{25}\text{Se}_{65}\text{Te}_{10}$ cladding layer, characterized by a refractive index of $n = 2.55 \pm 0.04$, and a $6\mu\text{m}$ -thick amorphous $\text{Ge}_{25}\text{Se}_{55}\text{Te}_{20}$ top core layer, characterized by a refractive index of $n = 2.65 \pm 0.04$, at the wavelength $\lambda = 1.55\ \mu\text{m}$. Subsequent photolithography using a mask consisting of several series of 17 strips of different widths (from 4 to $40\ \mu\text{m}$) followed by ion beam etching under a mixture of argon and oxygen provides surfaces composed of several chalcogenide waveguides, the distances between two successive waveguides being about $100\ \mu\text{m}$. Due to the used mask, the rib waveguides are characterized by different widths (from 4 to $40\ \mu\text{m}$), but each one consists in a trapezoidal guide of $4\mu\text{m}$ depth with angles of about 60° , as illustrated in Figure 1.

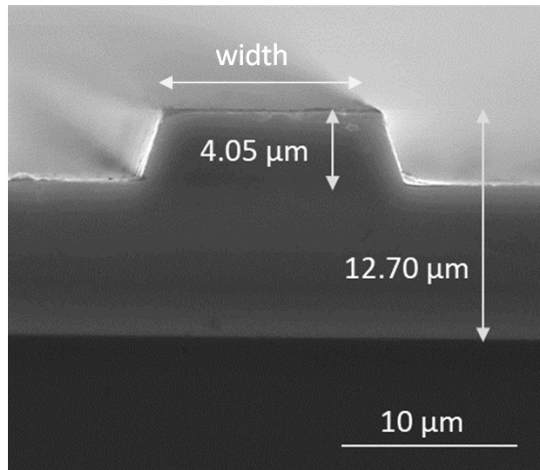


Figure 1. SEM image of a typical chalcogenide rib waveguide obtained by photolithography and ion beam etching. Note that it is not possible to distinguish between the two Ge-Se-Te layers, the sum of whose thicknesses is $12.7\ \mu\text{m}$.

In this work, our objective is to show the possibility of selectively functionalizing certain areas of the core layer. The buried cladding layer is essential to obtain a confinement of the light in the core layer, the refractive index of the silicon substrate being greater than that of the chalcogenide layers. On the other hand, it doesn't impact the surface properties of the waveguides. Therefore we simplified the waveguide fabrication process, by depositing only the core layer of $\text{Ge}_{25}\text{Se}_{55}\text{Te}_{20}$ composition on the silicon substrate. What we will call abusively the "waveguides" in the rest of the manuscript will be more precisely the slots formed after lithography and etching steps. In addition, we have modified the spreading conditions of the resist to achieve selective functionalization. After etching, a very thin layer of resist usually remains, which is typically removed by washing with acetone. In this work, the spin coating speed of the resist was

reduced from 4000 to 2000 rpm, that led to an increase in the resin thickness from 3 μm to 5 μm after the photolithographic step. In these conditions a subsequent and continuous layer of resist remained on the surface after the etching step, which was re-used as a mask for the further steps. Two strategies were then employed.

The first strategy aimed at functionalizing only the areas located between the “waveguides” as summarized in Figure 2. It consists in functionalization of the whole sample immediately after the ion etching, the residual resist still covering the top of the rib “waveguides”. After covalent modification of the Ge-Se-Te surface by organosilanes (described in the next paragraph), the residual resist was usually removed by acetone. Finally, the top of the “waveguide” was supposed to be unchanged, while to the surrounding areas were supposed to be functionalized.

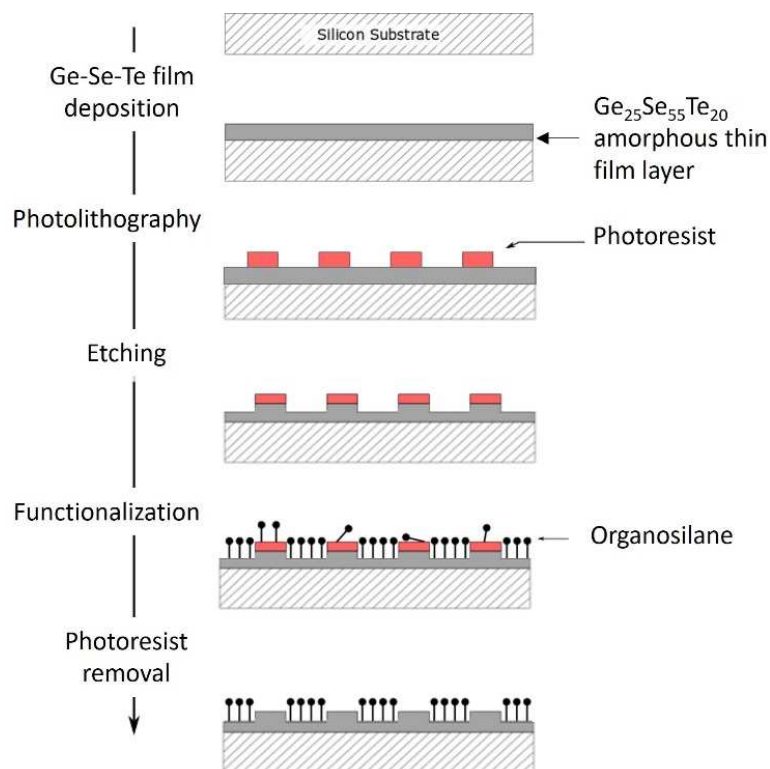


Figure 2. Process used to functionalize selectively the areas surrounding the rib “waveguides” (first strategy).

The second strategy aimed at functionalizing the rib “waveguides” alone. It involves the deposition of metallic sacrificial layer to invert the masked areas, as illustrated in Figure 3. Following the ion beam etching step, an aluminum nanometric sacrificial thin film was deposited by thermal evaporation in a vacuum chamber. An acetone rinse allows the aluminum-coated resin to be washed away, therefore providing unmasked “waveguides” surrounded by metal-masked areas. The silanization step was then carried on. Note that aluminum is expected to be also functionalized. Indeed, silanization of the aluminum

surface is straightforward, involving new Al-O-Si covalent groups [25;26]. Therefore, a last step consisting in a chemical etching was operated to remove the functionalized aluminum layer [27;28]. A diluted HCl aqueous solution was chosen as etchant because of its weak effect towards the organosilane layer, HCl being part of the precursor mixture. After few hours of etching in HCl at 1% (v/v), equivalent of 0.3 mol.L⁻¹, the thin Al film was fully dissolved. Finally, the top of the “waveguide” was supposed to be functionalized, while the surrounding areas were not.

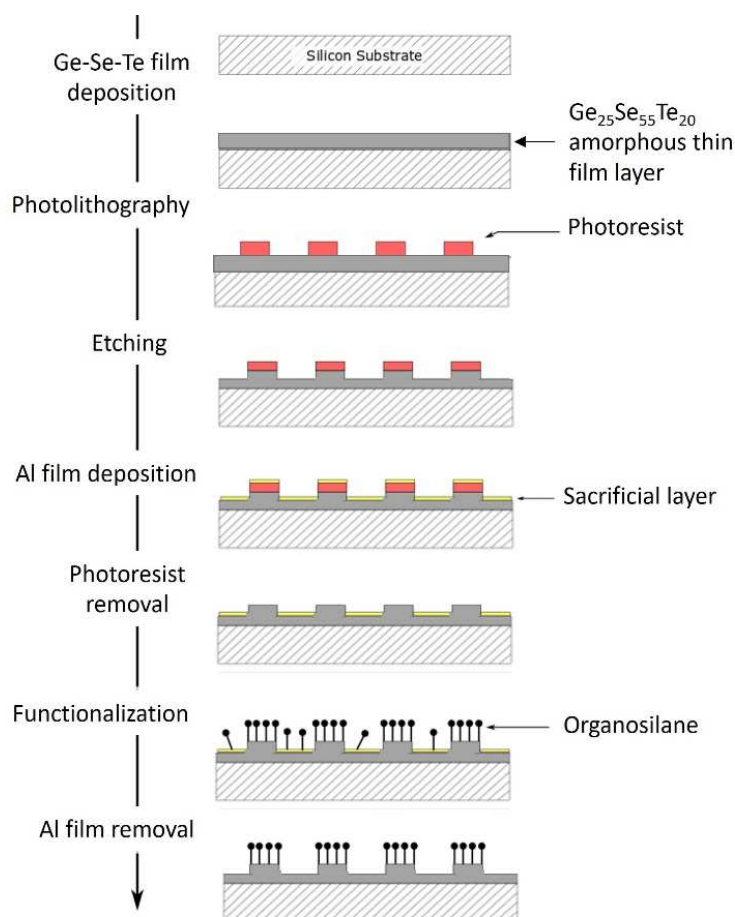


Figure 3. Process used to functionalize selectively the top of the rib “waveguides” (second strategy).

2.2. Surface functionalization

The functionalization process involved silanization of the Ge₂₅Se₅₅Te₂₀ core surface according to a protocol inspired from our previous work [29]. Three different organosilane precursors were used: (i) a fluorescent organosilane (triethoxysilyl fluorescein derivative), (ii) the tetraethoxysilane (TEOS) and (iii) a mixture of TEOS and octyl-trimethoxysilane (OTMS) [50:50], their structures being depicted in Figure 4. The fluorescent organosilane brings a fluorescent moiety (fluorescein) to be easily visualized on the

surface at the micrometric scale. Synthesis of this precursor is detailed in a previous work [30]. The most efficient excitation of the fluorescent moiety (fluorescein) being around 495 nm, the maximum emission occurs around 510 nm (Figure 4). The tetraethoxysilane (TEOS) and the mixture of tetraethoxysilane (TEOS) and octyl-trimethoxysilane (OTMS) were chosen to change the wettability of the chalcogenide surfaces. The surface of Ge-Se-Te layers is expected to become more hydrophilic after functionalization with the TEOS precursor, whereas it is expected to be more hydrophobic with the mixture of the two precursors TEOS + OTMS. Applying one or the other of the selective functionalization strategies must therefore make it possible to create a wettability contrast between the “waveguides” and the areas located between the “waveguides”.

For all the three precursor solutions, the chemical process is similar: the organosilane was diluted in a mixture of ethanol and acidic water [90:10] (v/v) at $10 \text{ mg}\cdot\text{ml}^{-1}$. The acidic environment provided by the hydrochloric acid ($\text{pH} = 1.5$) insured full hydrolysis of the precursor. The $\text{Ge}_{25}\text{Se}_{55}\text{Te}_{20}$ chalcogenide surface was first treated with an oxygen plasma aiming to create available hydroxyl groups, mainly in the forms of Te-OH and/or Ge-OH. Then the surface was dip-coated at a withdrawal speed of $20 \text{ cm}\cdot\text{min}^{-1}$; the thin liquid film was then allowed to dry at room temperature before curing at $80 \text{ }^\circ\text{C}$ for 3 hours. Condensations of both the hydroxyl groups on the $\text{Ge}_{25}\text{Se}_{55}\text{Te}_{20}$ surface and the organosilanes led to the establishment of a covalent linkage between the core material and the organosilane moiety.

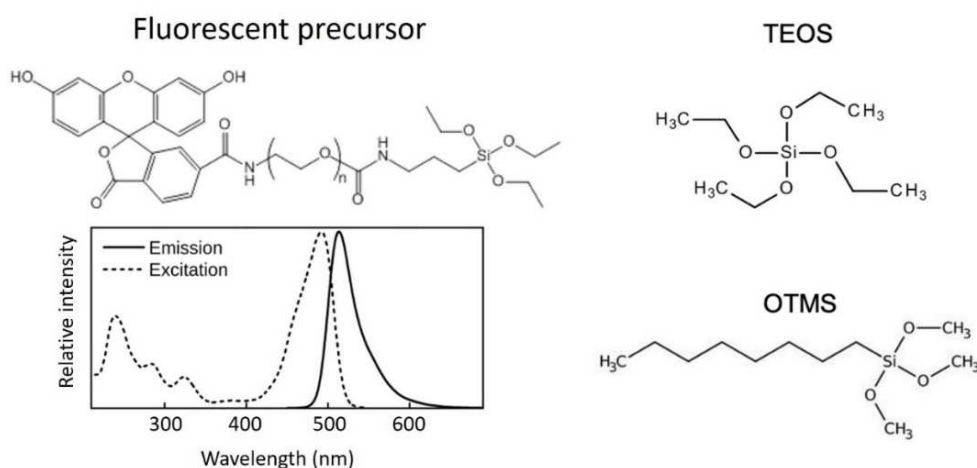


Figure 4. On the left: chemical structure; emission and excitation spectra of the triethoxysilyl fluorescein derivative, the fluorescent organosilane precursor we used [30]. On the right: chemical structures of the designed TEOS and OTMS organosilanes.

2.3. Surface characterization

The samples functionalized with the fluorescent precursor were imaged under a Nikon TE 2000 inverted microscope mounted by appropriate filters and dichroic mirrors to evidence the fluorescent signal emitted by the functionalized area.

The samples functionalized with TEOS or TEOS + OTMS were then characterized by Atomic Force Microscopy. AFM images were recorded in air using an Asylum Molecular Force Probe 3D head and a Molecular Force Probe 3D controller (from Asylum Research). Images were acquired in tapping mode using rectangular OMCL-AC240TS silicon cantilevers (Olympus) with a nominal tip radius of 7 nm. The height and phase images were recorded at 1Hz line-scan rate and digitized in 512×216 pixels at two different scan sizes ($40 \times 40 \mu\text{m}^2$ and $0.5 \times 0.5 \mu\text{m}^2$). The samples functionalized with TEOS or TEOS + OTMS were then characterized in terms of their wettability. The static water contact angle (WCA) values were measured for at least four different drops of 100 μL of distilled water using a SCA optical contact angle device and software.

2.4. Spore deposition

The strain *Magnaporthe oryzae* pv. FR94 was used for spore deposition tests. This fungus is a phytopathogenic Ascomycota responsible for rice blast, which is the most important disease affecting rice crops worldwide [31]. The strain was grown for 10 days on rice flour agar medium (20 g rice flour, 15 g agar, 2.5 g yeast extract, and 1L of distilled water) under fluorescent light (alternating white neon 3250 lumens and purple neon 1400) with a 12-hour photoperiod at 26 °C. Spores were then harvested by flooding the culture plates with 5 ml of sterile distilled water and filtering through a 22-25 μm Miracloth filter. The spore suspension was then spread on the different surfaces studied, with the spray nozzle providing spore dispersion. After 20 min of incubation, the surfaces were rinsed with 3 ml of distilled water. By counting the spores before and after the rinsing step, the rate of immobilized spores per unit area could be estimated.

3. Results

3.1. Evidencing the efficiency of the two selective functionalization strategies by fluorescent microscopy

To demonstrate the efficacy of the two proposed selective functionalization strategies, fluorescence microscopy imaging was performed on different surfaces: bare (images thus serving as reference), fully functionalized with the fluorescent organosilane, and partly functionalized with the fluorescent organosilane by applying either the first or the second strategy. First, in Figure 5 are presented the images obtained for a fully functionalized component (Figure 5.C) compared to that of a bare one (Figure 5.A). As expected, the non-functionalized surface does not exhibit any fluorescence (Figures 5.A and 5.B). On the contrary, the surface of the functionalized component is indeed fluorescent (Figure 5.C). This result is confirmed by the fluorescence intensity profile shown in Figure 5.D, where the intensity is non-zero whatever is the area of the component. However, as it can be seen in Figures 5.C and 5.D the fluorescence intensity is particularly high at the sidewalls of the “waveguides”. This can be explained by a higher binding site density provided by the non-horizontality and the higher rugosity of the sidewalls.

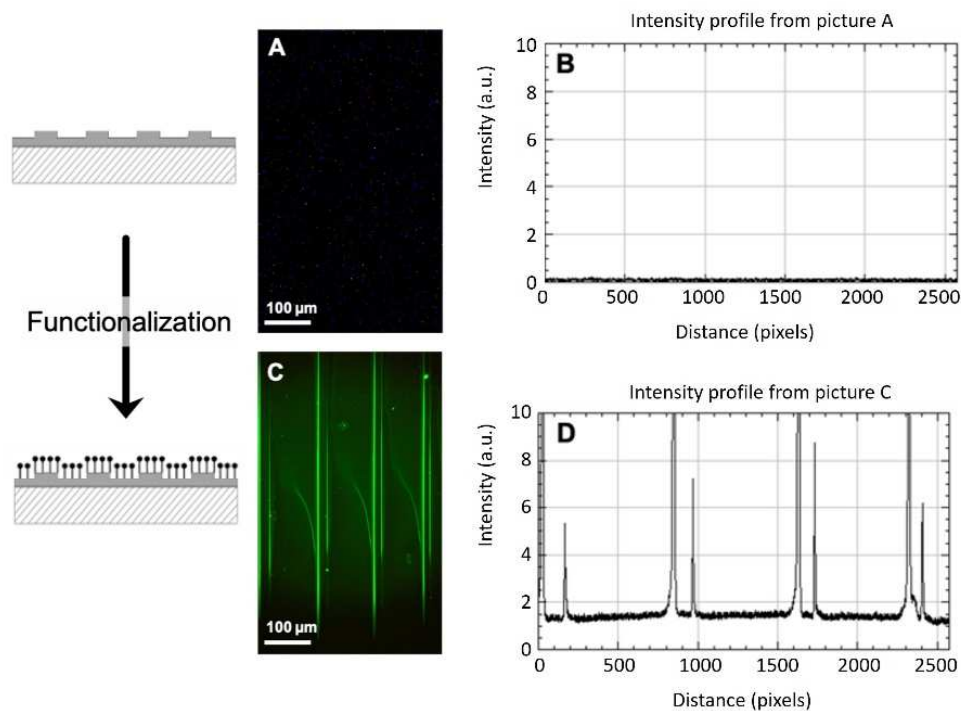


Figure 5. On the left: schemes of the analyzed components. In the middle: fluorescence microscope images of the component (A) before the functionalization step and (C) after functionalization of the full component. On the right: fluorescence intensity profiles of the corresponding surfaces: (B) before the functionalization step and (D) after functionalization of the full component.

In Figure 6 are compared the fluorescence images obtained for a component that has been functionalized according to the first strategy presented in Figure 2: (A) after the functionalization step and (C) after the cleaning step. Are also shown the corresponding fluorescence intensity profiles (Figures 6.B and 6.D). As highlighted by Figures 6.A and 6.B, the surface is fully fluorescent after functionalization, meaning that the fluorescent organosilane is bonded on both the etched Ge-Se-Te surface (between the “waveguides”) and on the photoresist (that is still on the top of the “waveguides”). After a cleaning step to remove the residual photoresist, one can observe in Figures 6.C and 6.D that only the areas between the “waveguides” are still fluorescent, as targeted by the first selective functionalization strategy. However, it can be noted that the sidewalls of the “waveguides” still fluoresce. This can be explained since the residual resin only protects the top of the “waveguides” during the functionalization step. Nevertheless, the functionalization operated selectively, creating a contrast between the top of the “waveguides” and the areas between the “waveguides”, demonstrating the appropriateness of the first proposed strategy.

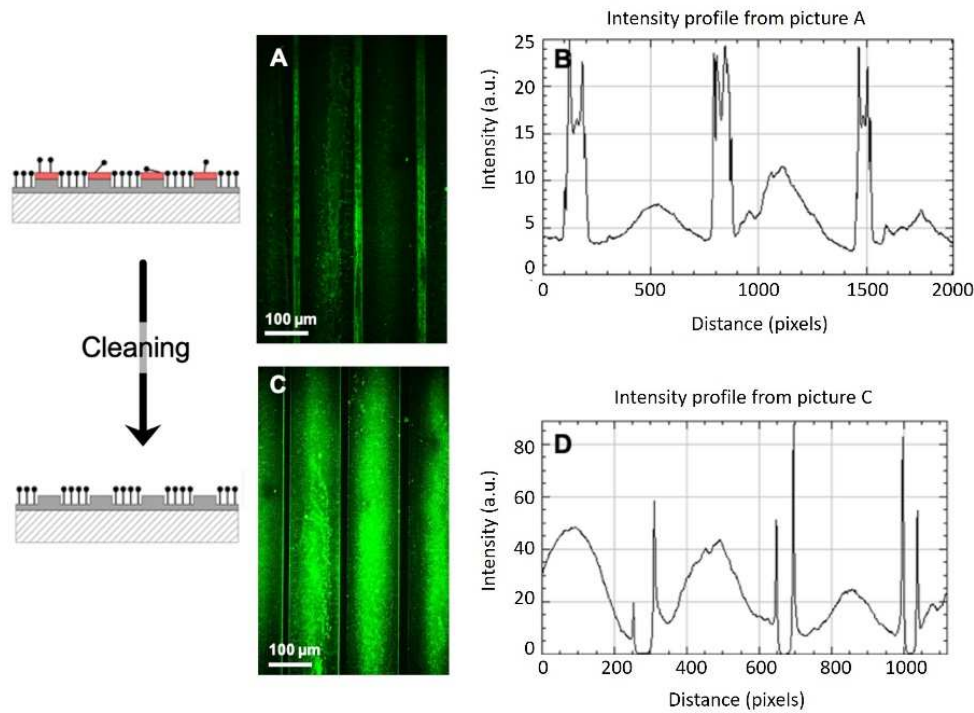


Figure 6. On the left: schemes of the analyzed components. In the middle: fluorescence microscope images of the component that has been functionalized according to the first strategy presented in Figure 2: (A) after the functionalization step and (C) after the photoresist removal. On the right: fluorescence intensity profiles of the corresponding surfaces: (B) after the functionalization step and (D) after the cleaning step.

In Figure 7 we compare the fluorescence images obtained for a component that has been functionalized according to the second strategy presented in Figure 3: (A) after the functionalization step and (C) after the aluminum etching step. The corresponding fluorescence intensity profiles are presented in Figures 7.B and 7.D. After functionalization the surface becomes fully fluorescent (Figures 7.A and 7.B), indicating that the fluorescent organosilane is bonded on both the top of the “waveguides” and between the “waveguides”, areas still covered by aluminum. The fluorescence intensity is nevertheless higher in the areas between the guides. This can be explained by the different optical properties of the metallic aluminum film and the glassy Ge-Se-Te film. Indeed, the Ge-Se-Te material would mainly absorb the visible light, while the aluminum would mainly reflect this light. It can also indicate that the functionalization was even more effective on the aluminum film than on the chalcogenide surface. According to the literature, the silanization of aluminum takes place via the creation of Al-O-Si covalent groups [25;32].

After the aluminum etching step, the fluorescence image (Figure 7.C) and the fluorescence intensity profile (Figure 7.D) depicts a new contrast. The brighter areas are localized on the waveguides, whereas a background signal is recorded from the surrounding areas. These results are consistent with those targeted by the second selective functionalization strategy, namely the selective functionalization of the “waveguides” and not the areas between them.

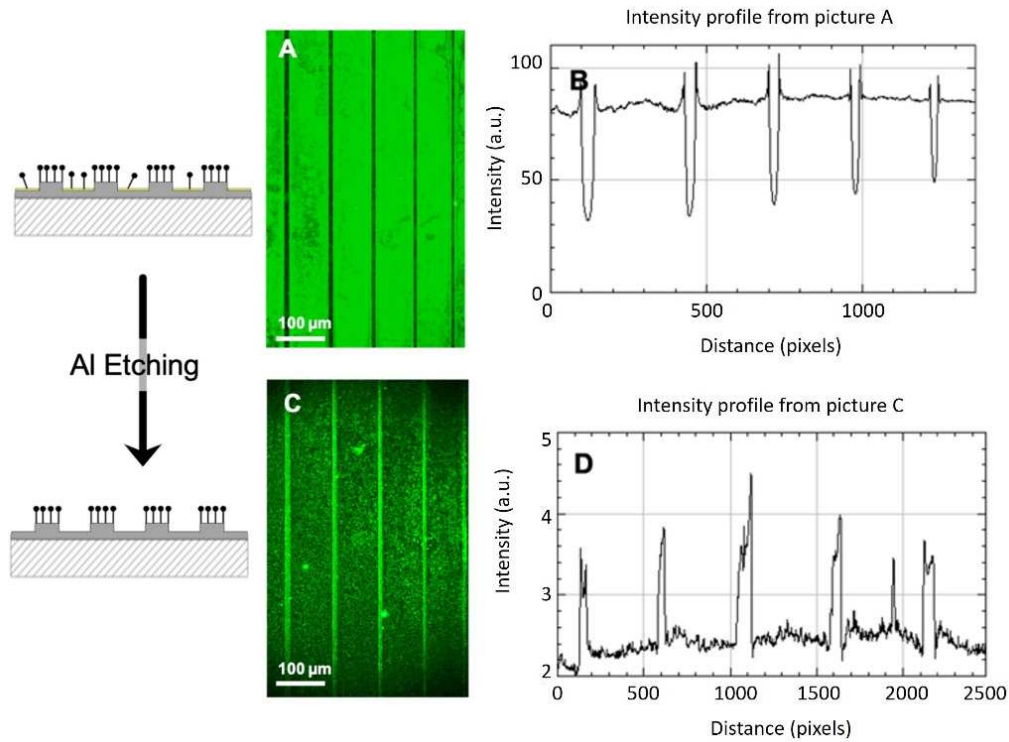


Figure 7. On the left: schemes of the analyzed components. In the middle: fluorescence microscope images of a component functionalized according to the second strategy presented in Figure 3: (A) after the functionalization step and (C) after the Al cleaning step. On the right: fluorescence intensity profiles of the corresponding surfaces: (B) after the functionalization step and (D) after the aluminum etching.

3.2. Application of the two selective functionalization strategies to create a wettability contrast

3.2.1. Nanoscale characterization of surfaces functionalized with TEOS by AFM

The surfaces functionalized with TEOS, according to one or the other of the two strategies, were analyzed by AFM. Height images (topographies) of the Ge-Se-Te surfaces obtained through the first strategy are displayed in Figure 8. The surface morphology is very different for the bare and functionalized areas, with large features on the bare $\text{Ge}_{25}\text{Se}_{55}\text{Te}_{20}$ (Figure 8, top left) and smaller ones on the silica functionalized area (Figure 8, top right). Roughness (RMS), extracted from those images, are also significantly different. The non-functionalized top waveguide area is smooth, with a roughness value (RMS) of 0.60 ± 0.10 nm,

while the functionalized area is rougher, with an RMS value reaching 0.85 ± 0.15 nm, probably due to the presence of the organosilane on the functionalized area.

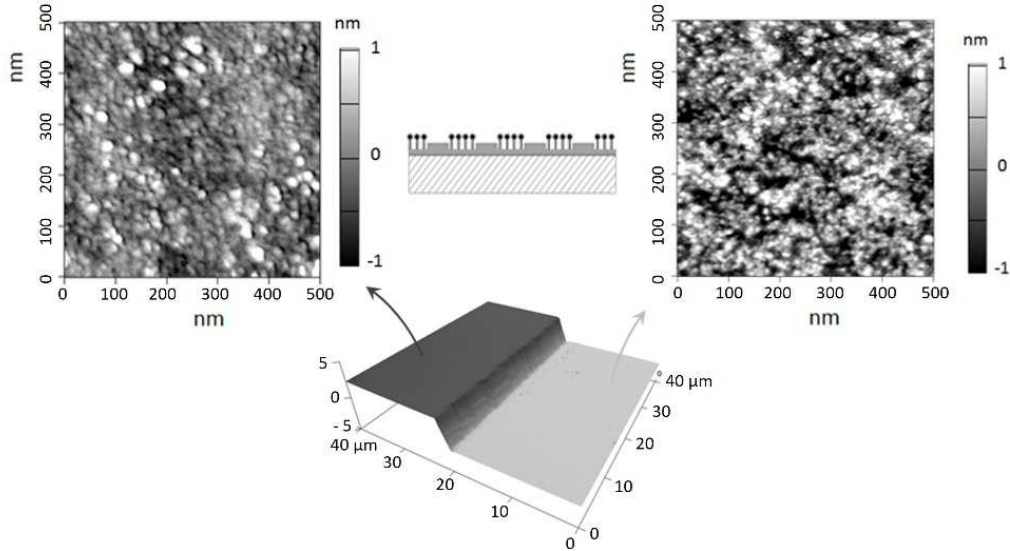


Figure 8. Below: AFM profile of a rib “waveguide”, after application of the first functionalization strategy with the TEOS precursor. Top left: AFM height image of the non-functionalized “waveguide”. Top right: AFM height image of the functionalized area.

Height images of the Ge-Se-Te surfaces obtained from the second strategy are displayed in Figure 9. Once again, the surface aspects are very different between bare and functionalized areas, with smaller asperities on the silica functionalized area (Figure 9, top left). This functionalized surface also exhibits large aggregates, probably due to the higher rate of TEOS homo-condensation [32;33]. Roughness extracted from those images, are also significantly different. The non-functionalized area between the “waveguides” is smooth, with an RMS value of 0.55 ± 0.10 nm, while the functionalized area is rougher, with RMS reaching 0.95 ± 0.15 nm.

This AFM analysis shows that the TEOS-functionalized areas exhibit smaller features, around several nanometers, also being significantly rougher compared to the non-functionalized areas. The effective anchor of the TEOS precursors to the chalcogenide materials probably explains these differences between bare and functionalized areas.

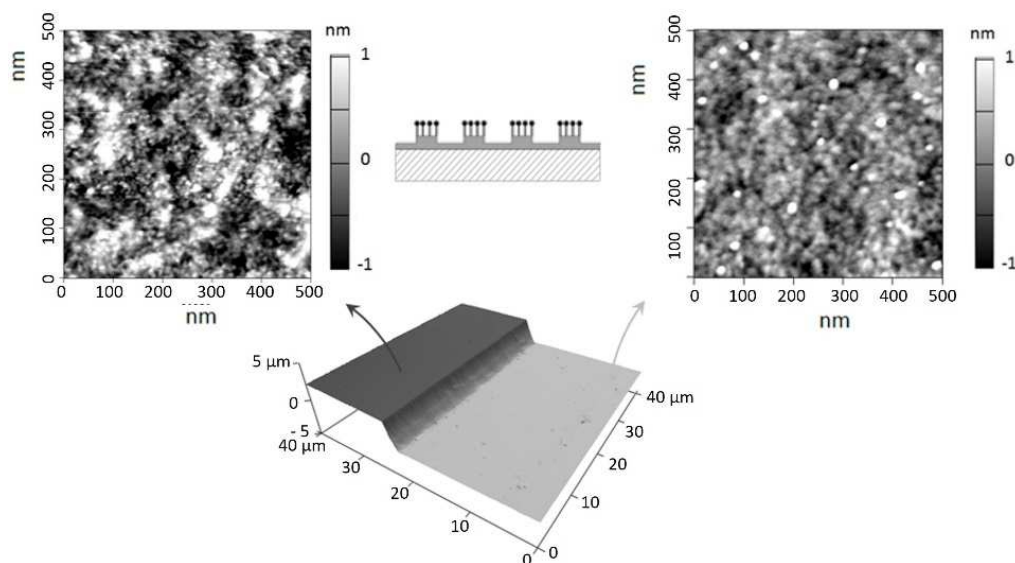


Figure 9. AFM profile of a rib “waveguide”, after application of the second functionalization strategy with the TEOS precursor. Top left: AFM height image of the functionalized “waveguide”. Top right: AFM height image of the non-functionalized surface.

3.2.2 Microscale characterization of surfaces functionalized with TEOS or TEOS + OTMS by WCA and observation of droplet edges

The water contact angle (WCA) technique gives us information about surface wettability: hydrophilic surfaces express low water contact angles ($< 90^\circ$), whereas hydrophobic surfaces express high contact angles ($> 90^\circ$). In our case, the TEOS precursor would provide more hydrophilic behavior thanks to hydroxyl groups (-OH) on the top surface [33]. On the other hand, adding the OTMS precursor would lead to more hydrophobic surface, due to the alkyl chains [32;35]. In Figure 10 are compared the water contact angles of the surfaces: functionalized with the TEOS precursor only (Figure 10, on the left) and functionalized with the mixture of the TEOS and OTMS precursors (Figure 10, on the right). Four differently modified surfaces are obtained: a non-functionalized component (serving as a reference), a full plate functionalized component (for comparison), a functionalized component obtained through the first strategy and second strategy, respectively. The diagrams below the graphs schematize these different surfaces. The surface of non-functionalized components is characterized by a water contact angle of $79 \pm 5^\circ$. Concerning the surfaces of full plate functionalized components, their WCA are of $47 \pm 5^\circ$ and $103 \pm 5^\circ$ when the precursor used is TEOS and TEOS + OTMS, respectively.

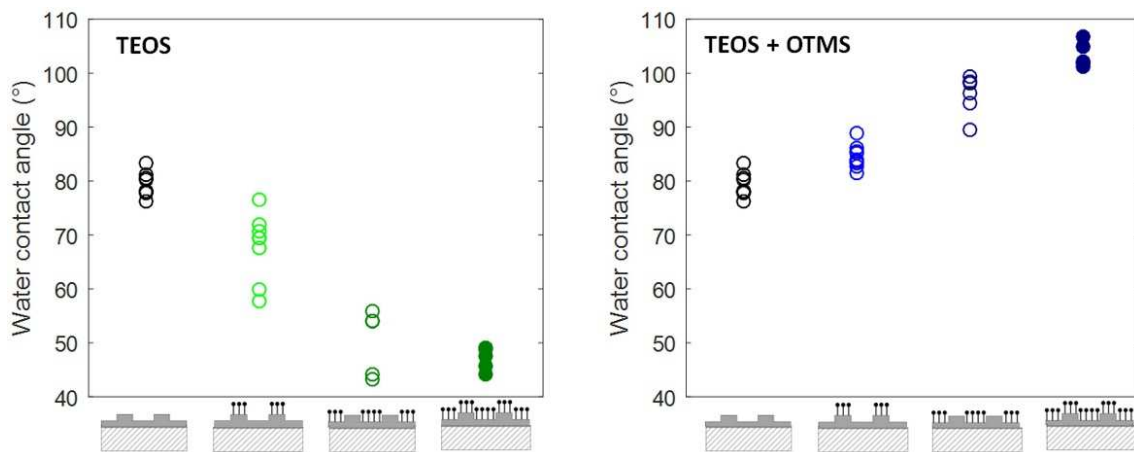


Figure 10. Water contact angles of four different surfaces using: the TEOS precursor (on the left); the TEOS + OTMS mixture (on the right). Below the graphs: scheme of the different surfaces: non-functionalized component, functionalized component according to the first strategy, functionalized component according to the second strategy and full plate functionalized component.

What can then be noticed in Figure 10 is that by applying our selective functionalization process, the measured contact angles are intermediate between those obtained for non-functionalized surfaces and those obtained for full plate functionalized surfaces. This was a predictable result since we only partially functionalized the surface. Moreover, one can see that the results obtained from measurements on the functionalized surfaces according to the second strategy are intercalated between those obtained from measurements on the non-functionalized surfaces and those obtained from measurements on the functionalized surfaces according to the first strategy. This result is coherent since the surface functionalized by the second method is less important than by the first method (the zones between the guides being predominant). These results confirm the effectiveness of the selective functionalization process applied to our surfaces.

To get a real insight to the microscale wettability characterization, pictures of the droplets edge have been recorded under a microscope. The pictures obtained for components according the first strategy, involving functionalization between the waveguides, are displayed in Figure 11. When the water droplet is deposited on the surface of a non-functionalized component, the contact is homogeneous with a smooth interface (Figure 11.A). Contrary, when the drop is deposited on the surface of a component where areas between the guides have been functionalized with the TEOS precursor, the contact is not homogeneous anymore, with larger contact with the functionalized areas, being more hydrophilic (Figure 11.B). When the drop is deposited on the surface of a component whose areas between the guides have been functionalized with the mixture of TEOS and OTMS precursors, again the contact is not homogeneous, but this time with a smaller contact with the functionalized areas, that had become more hydrophobic (Figure 11.C). This

simple observation demonstrates inhomogeneity in the surface wettability, coming from our selective functionalization process. In both cases (using TEOS or TEOS + OTMS), water maximizes its interaction with the most hydrophilic area, demonstrating the feasibility of the first strategy.

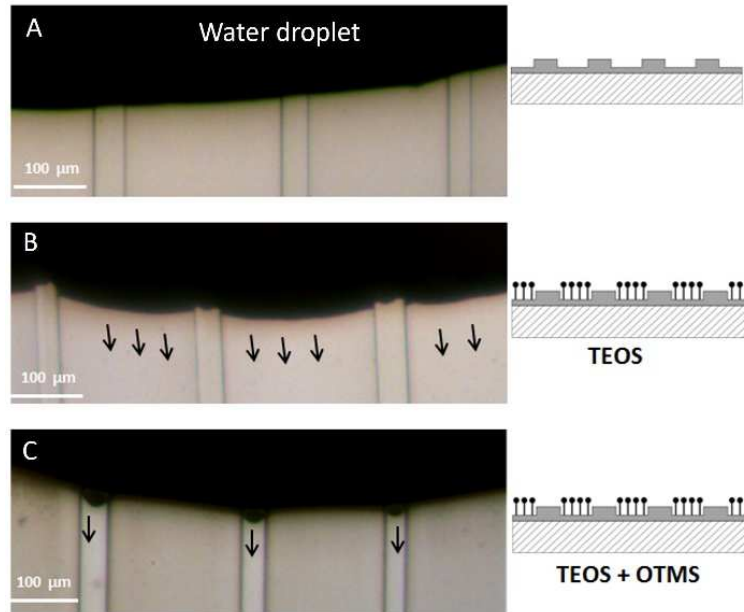


Figure 11. Optical observation of the front of a water drop deposited on three different surfaces: A) of a non-functionalized component; B) of a component functionalized with the TEOS precursor according to the first strategy; C) of a component functionalized with the TEOS + OTMS mixture according to the first strategy.

The pictures obtained on components issued from the second strategy, involving functionalization of “waveguides” only, are displayed in Figure 12. The differences observed according to which surface the drop was deposited on are much less pronounced than with the first strategy. This is because the “waveguides” are narrower than the areas between the waveguides. There is almost no difference in the drop front depending on whether the drop is deposited on a non-functionalized component (Figure 12.A) or if it is deposited on a component whose “waveguides” have been functionalized with the TEOS precursor (Figure 12.B). On the other hand, we can observe that the drop maximizes its contact with the areas located between the “waveguides” when they have been functionalized with the TEOS + OTMS mixture (Figure 12.C). This result confirms the efficiency of the second selective functionalization strategy.

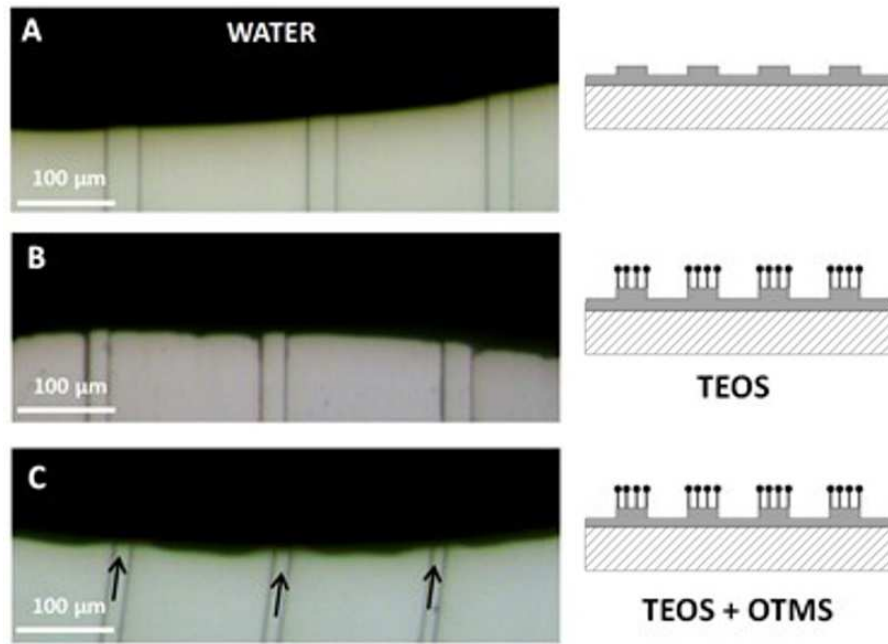


Figure 12. Optical observation of the front of a water drop deposited on three different surfaces: A) of a non-functionalized component; B) of a component functionalized with the TEOS precursor according to the second strategy; C) of a component functionalized with the TEOS + OTMS mixture according to the second strategy.

3.2.3 Components with wettability contrast: application to spore immobilization

To demonstrate the potential use of components presenting wettability contrast for early detection of fungal diseases, we've compared the immobilization rates of spores of phytopathogenic fungi on three different structures: a non-functionalized component, a component functionalized with the TEOS precursor according to the first strategy and one functionalized with the mixture of TEOS + OTMS precursors according to the second strategy. The spores of phytopathogenic fungi, responsible for the spread of fungal diseases are small hydrophobic cells that preferentially immobilize on hydrophobic surfaces [36], such as plant leaves. As a result, the rate of spores immobilized on the waveguides is expected to be greater for the two selectively functionalized components than for the non-functionalized component. Indeed, in the case of the selectively functionalized components, i.e., the component functionalized with the TEOS precursor according to the first strategy and the component functionalized with the TEOS + OTMS precursor mixture according to the second strategy, the wettability contrast is increased between the “waveguides” and the areas separating the “waveguides”.

Spores of *Magnaporthe oryzae* in solution were sprayed onto the surfaces of the three components. After evaporation of the solvent, we've counted the spores deposited on the waveguides (including the waveguide flanks), to determine the rate of spores sprayed per unit area. We then proceeded with a rinse,

with the objective of removing all unattached spores, dried the structures and we've counted again the spores present on the top and sides of the “waveguides”. This allowed us to calculate the rate of immobilized spores per unit area. The obtained rates of spores sprayed and immobilized per unit area are plotted in Figure 13 for the three components: the non-functionalized component, the component functionalized with the TEOS precursor according to the first strategy and the one functionalized with the TEOS + OTMS mixture according to the second strategy.

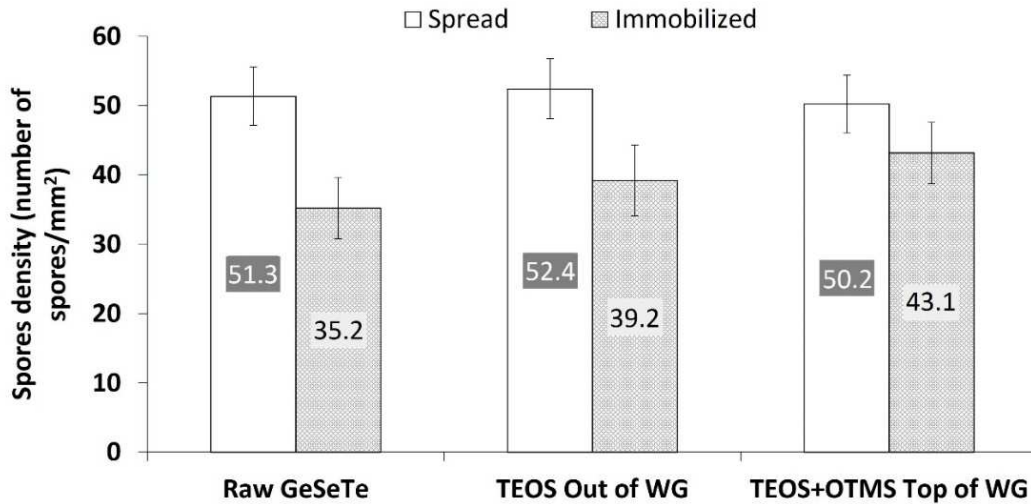


Figure 13: Spores density after spraying and rinsing for three different components: a non-functionalized component, a component functionalized with the TEOS precursor according to the first strategy and a component functionalized with the mixture of TEOS and OTMS according to the second strategy.

For all three components, approximately 50-52 spores.mm⁻² were sprayed onto the waveguides and their flanks, validating the homogeneity of the dispersion. For the reference, non-functionalized component, the value drops to 35.2 sp.mm⁻² after the rinsing step, meaning that a significant portion of the spores was washed away. For the other two components, all functionalization led to higher spore densities, reaching an average value of 39.2 and 43.1 sp.mm⁻² for the first and second strategy, respectively. In the first case, the spores sprayed on the areas between the guides were probably dislodged by the flushing, whereas for some the spores remained fixed on the sides of the “waveguides”. In the second case, spores sprayed on the waveguides were not removed by rinsing, attesting their affinity for the more hydrophobic surfaces. These results are consistent with our expectations and demonstrate the possible benefit of our two functionalization strategies.

It is important to emphasize that we made sure that it would be possible to regenerate the surfaces after spore attachment, without altering the functionalization. Since the interactions between spores and the

hybrid layer are weak (typically Van der Waals and hydrogen bonds), spores can be easily removed by simple washing with an appropriate solvent (ethanol, acetone, or surfactant for instance) giving rise to a surface with free ligands again. On the other hand, the organosilane functionalization of the chalcogenide involves strong covalent bonds, such as Ge-O-Si and Te-O-Si. Therefore, the washing process doesn't damage the hybrid layer. These washing processes were applied to our components, functionalized according to the first or the second strategy. Accordingly, all spores were removed from the surfaces using EtOH, acetone or SDS (sodium dodecyl sulfate), whereas the contact angles measured were the same before spore deposition and after cleaning.

Conclusion

We have proposed two new strategies for the functionalization of amorphous chalcogenide film-based sensors, allowing the selective functionalization of active (waveguides) or passive (areas surrounding the waveguides) areas of the optical sensing system. Both selective functionalization strategies consist in reusing the residual resist layer from the photolithography step as a mask during functionalization. The process is therefore relatively simple and adaptable to other materials. The choice of chalcogenide glasses is nevertheless judicious in the context of the realization of microsensors, the mid-infrared range being a spectral range relatively rich in information.

In this work, both selective functionalization processes were applied to samples consisting of a silicon substrate and a partially etched chalcogenide thin film, as it would be in a rib waveguide. They will be very easily transposable to real waveguides, requiring the deposition of an additional buffer layer, between the substrate and the core layer. The effectiveness of the two selective functionalization processes was first demonstrated using a fluorescent precursor, allowing functionalized areas to be easily distinguished from non-functionalized areas. The use of a hydrophilic precursor or a mixture of hydrophobic precursors was then used to create a wettability contrast between the functionalized and non-functionalized areas. The wettability contrast was then tested against the deposition of spores on the components. Spores are known in the literature to be preferentially immobilized to hydrophobic surfaces such as plant leaves. We therefore compared the immobilization rates of spores on our different surfaces. And indeed, the immobilization rate increased when the waveguides were made more hydrophobic (using the second strategy with the TEOS + OTMS mixture) or when the areas surrounding the waveguides were made more hydrophilic (using the first strategy with the TEOS precursor). In both cases, this means that the two functionalization strategies, used with the right precursor, can increase the rate of spores immobilized on our component. This is interesting if we plan to use these components as micro-sensors for early detection of plant diseases, via the detection of associated spores. This is interesting if we consider using these

components as microsensors for early detection of plant diseases, via detection of associated spores. It should be noted that without the organosilane layer, recent works have already shown that waveguides are sensitive to the presence of spores on their surface between 1.2 and 2 μm [37]. The changes at the output of the waveguide are small (about 0.02 %) but can be highlighted by multivariate analysis. Simulations carried out in parallel confirmed that the effect was weak in this wavelength range, where only scattering phenomena exists. By working further in the infrared, one can hope to “observe” the characteristic absorption bands of the spores and gain both in sensitivity and selectivity. To end, by making the waveguides more hydrophobic by applying the second strategy of selective functionalization described in this paper, the sensitivity should be increased. It should be stressed that a dip-coated organosilane layer has a thickness that does not exceed 100 nm. The evanescent field of the guiding structures as described in Figure 1 is present over a distance of the order of a micrometer at $\lambda = 1.55 \mu\text{m}$, a distance that increases with the wavelength. Interactions between the evanescent field and the spores will therefore be possible. To confirm this, future work will focus on simulations of the light/organosilane layer/spore interactions and on the corresponding optical characterizations.

Acknowledgments

This work was publicly funded through ANR (the French National Research Agency) under the “Investissements d’avenir” program with reference ANR-16-IDEX-0006. The authors are grateful to Sikémia company (Montpellier, France) for having kindly allowed us to use their plasma device.

References

- [1] Sharma, P.; Sharma, N.; Sharda, S.; Katyal, S. C. & Sharma, V., Recent developments on the optical properties of thin films of chalcogenide glasses, *Progress in Solid State Chemistry* (2016), 44(4), 131-141
- [2] Gai, X.; Han, T.; Prasad, A.; Madden, S.; Choi, D.-Y.; Wang, R.; Bulla, D. & Luther-Davies, B., Progress in optical waveguides fabricated from chalcogenide glasses, *Opt. Express* (2010), 18(25), 26635-26646
- [3] Eggleton, B. J., Chalcogenide photonics: fabrication, devices, and applications Introduction, *Optic Express* (2010), 18(25), 26632-26634
- [4] Kumar, A.; Shukla, S. & Shukla, R. K., Electrical, Photo-Electrical and Optical Properties of Selenium Rich Chalcogenide Glasses: A Review, *Material focus* 6 (2017), 6(44), 415-423

- [5] Su, P.; Han, Z.; Kita, D.; Becla, P.; Lin, H.; Deckoff-Jones, S.; Richardson, K.; Kimerling, L. C.; Hu, J. & Agarwal, A., Monolithic on-chip mid-IR methane gas sensor with waveguide-integrated detector, *Applied Physics Letters* (2019), 114(5), 051103
- [6] Charrier, J.; Brandily, M.-L.; Lhermite, H.; Michel, K.; Bureau, B.; Verger, F. & Nazabal, V., Evanescent wave optical micro-sensor based on chalcogenide glass, *Sensors and Actuators B: Chemical* (2012), 173, 468–476
- [7] Du, Q.; Luo, Z.; Zhong, H.; Zhang, Y.; Huang, Y.; Du, T.; Zhang, W.; Gu, T. & Hu, J., Chip-scale broadband spectroscopic chemical sensing using an integrated supercontinuum source in a chalcogenide glass waveguide, *Photon. Res.* (2018), 6(6), 506-510
- [8] Bendiab, A.; Ryckewaert, M.; Heran, D.; Escalier, R.; Kribich, R.; Vigreux, C. & Bendoula, R., Coupling Waveguide-Based Micro-Sensors and Spectral Multivariate Analysis to Improve Spray Deposit Characterization in Agriculture, *Sensors* (2019), 19, 4168
- [9] Gutierrez-Arroyo, A.; Baudet, E.; Bodiou, L.; Nazabal, V.; Rinnert, E.; Michel, K.; Bureau, B.; Colas, F. & Charrier, J., Theoretical study of an evanescent optical integrated sensor for multipurpose detection of gases and liquids in the Mid-Infrared, *Sensors and Actuators B: Chemical* (2017), 242, 842-848
- [10] Jin, T.; Zhou, J.; Lin, H.-Y. G. & Lin, P. T., Mid-Infrared Chalcogenide Waveguides for Real-Time and Nondestructive Volatile Organic Compound Detection, *Anal. Chem.* (2019), 91(1), 817-822
- [11] Vigreux, C.; Thi, M. V.; Maulion, G.; Kribich, R.; Barillot, M.; Kirschner, V. & Pradel, A., Wide range transmitting chalcogenide films and development of micro-components for infrared integrated optics applications, *Opt. Mater. Express* (2014), 4(8), 1617-1631
- [12] Ganjoo, A.; Jain, H.; Yu, C.; Song, R.; Ryan, J. V.; Irudayaraj, J.; Ding, Y. J. & Pantano, C. G., Planar chalcogenide glass waveguides for IR evanescent wave sensors, *Journal of Non-Crystalline Solids* (2006), 352(6), 584-588
- [13] Taleb Bendiab, A.; Bathily, M.; Vigreux, C.; Escalier, R.; Pradel, A.; Kribich, R. & Bendoula, R., Chalcogenide rib waveguides for the characterization of spray deposits, *Optical Materials* (2018), 86, 298-303
- [14] Vigreux, C.; Thi, M. V.; Escalier, R.; Maulion, G.; Kribich, R. & Pradel, A., Channel waveguides based on thermally co-evaporated Te–Ge–Se films for infrared integrated optics, *Journal of Non-Crystalline Solids* (2013), 377(1-5), 205-208

- [15] Hu, J.; Tarasov, V.; Carlie, N.; Feng, N.-N.; Petit, L.; Agarwal, A.; Richardson, K. & Kimerling, L., Si-CMOS-compatible lift-off fabrication of low-loss planar chalcogenide waveguides, *Opt. Express* (2007), 15(19), 11798-11807
- [16] Singh, V.; Lin, P. T.; Patel, N.; Lin, H.; Li, L.; Zou, Y.; Deng, F.; Ni, C.; Hu, J.; Giammarco, J.; Soliani, A. P.; Zdyrko, B.; Luzinov, I.; Novak, S.; Novak, J.; Wachtel, P.; Danto, S.; Musgraves, J. D.; Richardson, K.; Kimerling, L. C. & Agarwal, A. M., Mid-infrared materials and devices on a Si platform for optical sensing, *Science and Technology of Advanced Materials* (2014), 15(1), 014603
- [17] Martín-Palma, R. J.; Demirel, M. C.; Wang, H. & Pantano, C. G., Surface biofunctionalization of nanostructured GeSbSe chalcogenide glass thin films, *Journal of Non-Crystalline Solids* (2009), 355(3), 208-212
- [18] Han, Z.; Lin, P.; Singh, V.; Kimerling, L.; Hu, J.; Richardson, K.; Agarwal, A. & Tan, D. T. H., On-chip mid-infrared gas detection using chalcogenide glass waveguide, *Applied Physics Letters* (2016), 108(14), 141106
- [19] Ma, P.; Choi, D.-Y.; Yu, Y.; Gai, X.; Yang, Z.; Debbarma, S.; Madden, S. & Luther-Davies, B., Low-loss chalcogenide waveguides for chemical sensing in the mid-infrared, *Opt. Express* (2013), 21(24), 29927-29937
- [20] Li, W.; Anantha, P.; Lee, K. H.; Qiu, H. D.; Guo, X.; Goh, S. C. K.; Zhang, L.; Wang, H.; Soref, R. A. & Tan, C. S., Spiral Waveguides on Germanium-on-Silicon Nitride Platform for Mid-IR Sensing Applications, *IEEE Photonics Journal* (2018), 10(3), 1-7
- [21] Madden, S. J.; Choi, D.-Y.; Bulla, D. A.; Rode, A. V.; Luther-Davies, B.; Ta'eed, V. G.; Pelusi, M. D. & Eggleton, B. J., Long, low loss etched As₂S₃ chalcogenide waveguides for all-optical signal regeneration. In: *Opt. Express* (2007), 15(22), 14414-14421
- [22] Carlie, N.; Musgraves, J. D.; Zdyrko, B.; Luzinov, I.; Hu, J.; Singh, V.; Agarwal, A.; Kimerling, L. C.; Canciamilla, A.; Morichetti, F.; Melloni, A. & Richardson, K., Integrated chalcogenide waveguide resonators for mid-IR sensing: leveraging material properties to meet fabrication challenges, *Opt. Express* (2010), 18(25), 26728-26743
- [23] Hu, J.; Feng, N.-N.; Carlie, N.; Petit, L.; Agarwal, A.; Richardson, K. & Kimerling, L., Optical loss reduction in high-index-contrast chalcogenide glass waveguides via thermal reflow, *Optics express* (2010), 18, 1469-1478
- [24] Terhune, B.T. and Hoch H.V, Substrate hydrophobicity and adhesion of *Uromyces* Urediospores and Germlings, *Experimental Mycology* (1993), 17, 241-252

- [25] Zhang, X.; Yue, W.; You, Y. & Luo, S., Silane Treatment Technology on Aluminum Surface, *Advanced Materials Research* (2011), 239-242, 2687-2693
- [26] Milosev, I.; Jovanović, Z.; Bajat, J. B.; Jancić-Heinemann, R. & Misković-Stanković, V. B., Surface Analysis and Electrochemical Behavior of Aluminum Pretreated by Vinyltriethoxysilane Films in Mild NaCl Solution, *Journal of The Electrochemical Society* (2012), 159(7), C303-C311
- [27] Oh, H.-J.; Lee, J.-H.; Ahn, H.-J.; Jeong, Y.; Park, N.-J.; Kim, S.-S. & Chi, C.-S., Etching characteristics of high-purity aluminum in hydrochloric acid solutions, *Materials Science and Engineering: A* (2007), 449-451(3), 348-351
- [28] Yildiz, M., Investigation of Etchants for Etching Conditions of Aluminium, *International Journal of Scientific and Technological Research* (2016), 2(3), 1-9
- [29] Robert, B.; Martin, M.; Escalier, R.; Varga, B.; Mehdi, A.; Vigreux, C. & Gergely, C., Strategies for Chalcogenide Thin Film Functionalization, *Langmuir* (2020), 36(26), 7691-7700
- [30] Echaliier, C.; Pinese, C.; Garric, X.; Van Den Berghe, H.; Jumas Bilak, E.; Martinez, J.; Mehdi, A. & Subra, G., Easy Synthesis of Tunable Hybrid Bioactive Hydrogels, *Chem. Mater.* (2016), 28(5), 1261-1265
- [31] Fernandez, J. & Orth, K., Rise of a Cereal Killer: The Biology of *Magnaporthe oryzae* Biotrophic Growth, *Trends in Microbiology* (2018), 26(7), 582–597
- [32] Agbe, H.; Sarkar, D. K. & Chen, X.-G., Tunable Superhydrophobic Aluminum Surfaces with Anti-Biofouling and Antibacterial Properties, *Coatings* (2020), 10(10), 982
- [33] Yang, X.; Zhu, L.; Chen, Y.; Bao, B.; Xu, J. & Zhou, W., Controlled hydrophilic/hydrophobic property of silica films by manipulating the hydrolysis and condensation of tetraethoxysilane, *Applied surface science* (2016), 376, 1-9
- [34] Peeters, M. P. J., Bernards, T. N. M. & Van Bommel, M. J., O-17-NMR of sol-gel processes of TEOS and TMOS, *Journal of sol-gel science and technology* (1998), 13(1-3), 71-74.
- [35] Purcar, V.; Cinteza, O.; Ghiurea, M.; Balan, A.; Caprarescu, S. & Donescu, D. A. N., Influence of hydrophobic characteristic of organo-modified precursor on wettability of silica film. In: *Bulletin of Material science* (2014), 37, 107-115
- [36] Epstein L. and Nicholson R., Adhesion and Adhesives of Fungi and Oomycetes, Springer (Hrsg.): *Springer International* (2016), 25-55

- [37] Robert B., Functionalization of chalcogenide waveguides for the detection of phytopathogenic spores, Thesis, University of Montpellier (November 2021)